A Second-Order Reliability Method With First-Order Efficiency

Junfu Zhang
School of Mechanical Engineering,
Xihua University,
Chengdu 610039, P.R. China
e-mail: zhangjun@mst.edu

Xiaoping Du[1]
Department of Mechanical and Aerospace Engineering,
Missouri University of Science and Technology
e-mail: dux@mst.edu

The first-order reliability method (FORM) is efficient but may not be accurate for nonlinear limit-state functions. The second-order reliability method (SORM) is more accurate but less efficient. To maintain both high accuracy and efficiency, we propose a new second-order reliability analysis method with first-order efficiency. The method first performs the FORM to identify the most probable point (MPP). Then, the associated limit-state function is decomposed into additive univariate functions at the MPP. Each univariate function is further approximated by a quadratic function. The cumulant generating function of the approximated limit-state function is then available so that saddlepoint approximation can be easily applied in computing the probability of failure. The accuracy of the new method is comparable to that of the SORM, and its efficiency is in the same order of magnitude as the FORM. [DOI: 10.1115/1.4002459]

1 Introduction

The major task of reliability analysis is to compute the probability of failure p_f

$$p_f = \Pr\{g(\mathbf{X}) < q\} \tag{1}$$

where $g(\mathbf{X})$ is a limit-state function, $\mathbf{X}$ is a vector of random variables, and q is a limit state.

Accurately calculating p_f is computationally expensive, and therefore approximations are needed. The popular approximation methods include the advanced mean value method [1], the first-order reliability method (FORM) [2,3], and the second-order reliability method (SORM) [4]. The FORM is most commonly used because it is efficient; its accuracy, however, deteriorates when the nonlinearity of limit-state functions increases. The SORM overcomes this drawback with a cost of lower efficiency.

The purpose of this work is to improve the accuracy of the FORM. The new method builds on several existing techniques, such as the univariate dimension reduction [5–13] and the saddlepoint approximation [14]. Some of these methods are briefly reviewed below.

In Ref. [11], $g(\mathbf{X})$ is approximated at the most probable point (MPP) with higher-order univariate functions, and then Monte Carlo simulation (MCS) is used to evaluate p_f; the maximum number of limit-state function calls, in addition to that for the MPP search, is $mn+1$, where m is the order of the approximation and n is the number of random variables. To avoid using MCS, the same research group proposes to use the second-order univariate functions so that p_f can be estimated with numerical integration [13]. To make the numerical integration tractable, the authors first use transformations, such as the Gram–Schmidt orthogonalization, and then employ the univariate dimension reduction again to approximate the multidimensional probability integration. The number of function calls also depends on the number of integration points and the number of random variables. In Ref. [14], the bivariate dimension reduction and numerical integrations are used to approximate the first four statistical moments of $g(\mathbf{X})$. Then, the saddlepoint approximation is used to estimate p_f. Although the method is accurate without any MPP search, it is relatively expensive. If the number of the integration points is 3 for the moment estimation, the cost of the method is $9n(n-1)/2+3n+1$.

In this work, we propose a second-order reliability method with first-order efficiency (SORM-FOE). It searches for the MPP and then decomposes the limit-state function at the MPP into univariate functions. Each univariate function is further approximated into a quadratic function. The SORM-FOE is, in general, more accurate than the FORM. It needs only n more function calls than the FORM and still has the first-order efficiency.

This paper is organized as follows: The FORM and SORM are briefly reviewed in Sec. 2. The proposed SORM-FOE is discussed in Sec. 3. Examples are given in Sec. 4 followed by conclusions in Sec. 5.

2 Review of the FORM and SORM

2.1 FORM. The FORM [2,3,15–26] linearizes $g(\mathbf{X})$ at the MPP in the transformed U-space, which consists of independent standard normal variables $\mathbf{U}$ that are transformed from independent random variables $\mathbf{X}$. The transformation is given by [17,27]

$$F_{X_i}(X_i) = \Phi(U_i) \tag{2}$$

where F_{X_i} and Φ are the cumulative distribution functions (CDF) of X_i and U_i, respectively,

$$U_i = \Phi^{-1}\{F_i(X_i)\} \tag{3}$$

If X_i $(i=1,\ldots,n)$ are dependent, the transformation is given by the Nataf transformation [27],

$$\begin{aligned} U_1 &= \Phi^{-1}\{F_{X1}(X_1)\} \\ U_2 &= \Phi^{-1}\{F_{X2|X_1}(X_2|X_1)\} \\ U_3 &= \Phi^{-1}\{F_{X3|X_1,X_2}(X_3|X_1,X_2)\} \\ &\cdots \end{aligned} \tag{4}$$

where $F_{X2|X_1}(X_2|X_1)$ and $F_{X3|X_1,X_2}(X_3|X_1,X_2)$ are conditional CDFs of X_2 and X_3, respectively.

The MPP $\mathbf{u}^*$ is found by solving

[1]Corresponding author.

Contributed by the Design Automation Committee of ASME for publication in the JOURNAL OF MECHANICAL DESIGN. Manuscript received April 9, 2010; final manuscript received August 7, 2010; published online October 4, 2010. Assoc. Editor: Michael Kokkolaras.

 Copyright © 2010 by ASME

Downloaded From: http://mechanicaldesign.asmedigitalcollection.asme.org/ on 01/12/2016 Terms of Use: http://www.asme.org/about-asme/terms-of-use

$$\min \quad \|\mathbf{u}\| = \sqrt{\sum_{i=1}^{n} u_i^2}$$
$$\text{subject to} \quad \hat{g}(\mathbf{u}) = q \tag{5}$$

where $\hat{g}(\cdot)$ is the limit-state function in the U-space. Then, the reliability index is calculated by

$$\beta = \|\mathbf{u}^*\| = \left[\sum_{i=1}^{n} (u_i^*)^2\right]^{1/2} \tag{6}$$

When $p_f < 0.5$, p_f is computed by [28]

$$p_f = \Phi(-\beta) \tag{7}$$

A MPP search algorithm may need the derivatives of $\hat{g}(\mathbf{U})$ [29]. If the derivatives are evaluated numerically, the number of function calls will be linearly proportional to the number of random variables n. If the forward finite difference algorithm is used, the number of limit-state function calls N_{FORM} is

$$N_{\text{FORM}} = k(n+1) \tag{8}$$

where k is the number of iterations of the MPP search. Because N_{FORM} is linear in terms of n, the FORM is first-order efficient.

2.2 SORM. If $\hat{g}(\mathbf{U})$ is highly nonlinear, the FORM will be inaccurate. Then, the SORM may be used. Breitung's formulation [4] for the SORM is given by

$$p_f = \Phi(-\beta)\prod_{i=1}^{n-1}(1+\beta v_i)^{1/2} \tag{9}$$

where v_i $(i=1,\ldots,n-1)$ are the principal curvatures of $\hat{g}(\mathbf{U})$ at the MPP. The other popular SORM formulation is given by Tvedt [30], which is considered more accurate than the Breitung's formulation [31].

The SORM is more expensive than the FORM because second derivatives are required. If the forward finite difference formula is used for the derivative evaluation, the number of function calls by the SORM is

$$N_{\text{SORM}} = k(n+1) + \frac{n(n+1)}{2} = N_{\text{MPP}} + \frac{n(n+1)}{2} \tag{10}$$

The SORM is second-order efficient because N_{SORM} is quadratic in terms of n.

3 The Second-Order Reliability Method With First-Order Efficiency

3.1 Procedure. As mentioned previously, the proposed SORM-FOE improves the accuracy of the FORM while maintaining a similar level of efficiency. This is achieved by approximating $\hat{g}(\mathbf{U})$ with univariate functions, which are further approximated into quadratic forms. The method is outlined in Fig. 1, and its steps are explained below.

3.2 MPP Search. The MPP $\mathbf{u}^*$ is obtained by solving

$$\min \quad \|\mathbf{u}\| = \sqrt{\sum_{i=1}^{n} u_i^2}$$
$$\text{subject to} \quad \hat{g}(\mathbf{u}) = q \tag{11}$$

Optimization algorithms or MPP search algorithms [29] can be used to solve for the MPP.

3.3 Approximation of $\hat{g}(\mathbf{U})$. We now approximate $\hat{g}(\mathbf{U})$ at the MPP $\mathbf{u}^*$ with additive univariate functions [5–10],

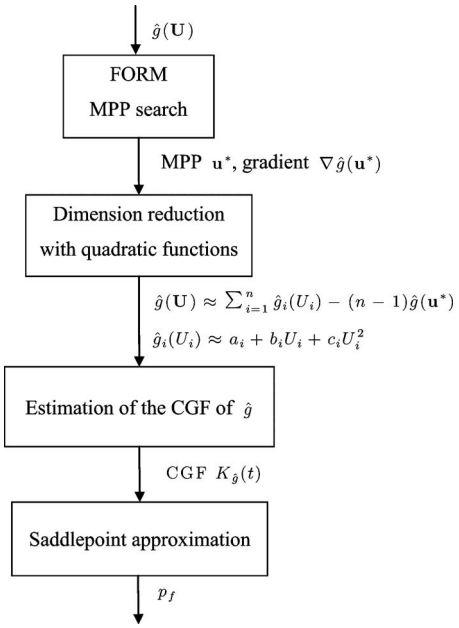

Fig. 1 Flowchart of SORM-FOE

$$\hat{g}(\mathbf{U}) \approx \sum_{i=1}^{n}\hat{g}_i(U_i) - (n-1)\hat{g}(\mathbf{u}^*) \tag{12}$$

where

$$\hat{g}_i(U_i) = \hat{g}(u_1^*, u_2^*, \ldots, u_{i-1}^*, U_i, u_{i+1}^*, \ldots, u_n^*) \tag{13}$$

which is a univariate function of U_i $(i=1,\ldots,n)$. The term $(n-1)\hat{g}(\mathbf{u}^*)$ makes the approximation exact at $\mathbf{u}^*$. We then approximate the function with a second-order polynomial in the form of

$$\hat{g}_i(U_i) \approx a_i + b_iU_i + c_iU_i^2 \tag{14}$$

From the MPP search, we have obtained the MPP $\mathbf{u}^*$ and the gradient of $\hat{g}(\mathbf{U})$, $\nabla\hat{g}(\mathbf{u}^*)$. We can use them to determine the coefficients a_i, b_i, and c_i in Eq. (14). The gradient $\nabla\hat{g}(\mathbf{u}^*)$ is given by

$$\nabla\hat{g}(\mathbf{u}^*) = \left.\left(\frac{\partial\hat{g}(\mathbf{U})}{\partial U_1}, \frac{\partial\hat{g}(\mathbf{U})}{\partial U_2}, \cdots, \frac{\partial\hat{g}(\mathbf{U})}{\partial U_n}\right)\right|_{\mathbf{u}^*} \tag{15}$$

Form Eq. (13), we have

$$\left.\frac{d\hat{g}_i(U_i)}{dU_i}\right|_{u_i^*} = \left.\frac{\partial\hat{g}(U)}{\partial U_i}\right|_{\mathbf{u}^*} \tag{16}$$

We then need one more point to determine a_i, b_i, and c_i. We call this new point $\tilde{u}_i$, and it is on the U_i-axis, as shown in Fig. 2. $\tilde{u}_i$ is determined by a step size δ_i and is given by

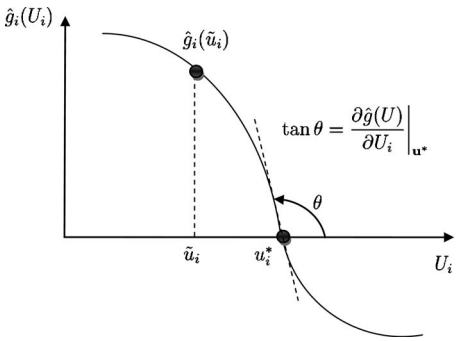

Fig. 2 Information used for approximation

Downloaded From: http://mechanicaldesign.asmedigitalcollection.asme.org/ on 01/12/2016 Terms of Use: http://www.asme.org/about-asme/terms-of-use

$$\tilde{u}_i = u_i^* + \delta_i \tag{17}$$

where u_i^* is the ith component of the MPP.

At $\tilde{u}_i$, $\tilde{g}_i(\tilde{u}_i)$ is given by

$$\tilde{g}_i(\tilde{u}_i) = \hat{g}(u_1^*, u_2^*, \ldots, u_{i-1}^*, \tilde{u}_i, u_{i+1}^*, \ldots, u_n^*) \tag{18}$$

Since

$$\left.\frac{\partial \hat{g}(U)}{\partial U_i}\right|_{\mathbf{u}^*} = \left.\frac{\mathrm{d}\hat{g}_i(U_i)}{\mathrm{d}U_i}\right|_{u_i^*} = b_i + 2c_i u_i^*$$

the coefficients can be solved by

$$\begin{bmatrix} 1 & u_i^* & (u_i^*)^2 \\ 1 & \tilde{u}_i & (\tilde{u}_i)^2 \\ 0 & 1 & 2u_i^* \end{bmatrix} \begin{bmatrix} a_i \\ b_i \\ c_i \end{bmatrix} = \begin{bmatrix} q \\ \hat{g}_i(\tilde{u}_i) \\ \left.\dfrac{\partial \hat{g}(U)}{\partial U_i}\right|_{\mathbf{u}^*} \end{bmatrix} \tag{19}$$

where q is the limit state defined in Eq. (1). After solving for a_i, b_i, and c_i from Eq. (19), we obtain $\hat{g}_i(U_i)$ as

$$\begin{aligned} \hat{g}_i(U_i) &\approx \begin{cases} \left(\sqrt{c_i}U_i + \dfrac{1}{2}\dfrac{b_i}{\sqrt{c_i}}\right)^2 + a_i - \dfrac{b_i^2}{4c_i} & c_i > 0 \\ -\left(\sqrt{-c_i}U_i - \dfrac{1}{2}\dfrac{b_i}{\sqrt{-c_i}}\right)^2 + a_i - \dfrac{b_i^2}{4c_i} & c_i < 0 \\ a_i + b_i U_i & c_i = 0 \end{cases} \\ &= \begin{cases} e_i + Z_i^2 & c_i > 0 \\ e_i - Z_i^2 & c_i < 0 \\ a_i + b_i U_i & c_i = 0 \end{cases} \end{aligned} \tag{20}$$

where

$$e_i = a_i - \frac{b_i^2}{4c_i} \tag{21}$$

and

$$Z_i = \begin{cases} \sqrt{c_i}U_i + \dfrac{1}{2}\dfrac{b_i}{\sqrt{c_i}} & c_i > 0 \\ \sqrt{-c_i}U_i - \dfrac{1}{2}\dfrac{b_i}{\sqrt{-c_i}} & c_i < 0 \end{cases} \tag{22}$$

Because Z_i is a linear function of U_i, it also follows a normal distribution $N(\mu_{Z_i}, \sigma_{Z_i})$, where

$$\mu_{Z_i} = \begin{cases} \dfrac{1}{2}\dfrac{b_i}{\sqrt{c_i}} & c_i > 0 \\ -\dfrac{1}{2}\dfrac{b_i}{\sqrt{-c_i}} & c_i < 0 \end{cases} \tag{23}$$

and

$$\sigma_{Z_i} = \begin{cases} \sqrt{c_i} & c_i > 0 \\ -\sqrt{-c_i} & c_i < 0 \end{cases} \tag{24}$$

3.4 CGF of $\hat{g}(\mathbf{U})$. After decomposing $\hat{g}(\mathbf{U})$, we now derive its cumulant generating function (CGF). With the CGF, we can then obtain p_f without any numerical integration. According to Ref. [32], $(Z_i/\sigma_{Z_i})^2$ follows a noncentral chi-square distribution with freedom of 1; namely, $(Z_i/\sigma_{Z_i})^2 \backsim \chi^2(1, \lambda)$, where

$$\lambda = \frac{\mu_{Z_i}}{\sigma_{Z_i}} \tag{25}$$

The CGF of $(Z_i/\sigma_{Z_i})^2$ is given by

$$K_{Z_i}(t) = \frac{\lambda_i t}{1-2t} - \frac{1}{2}\log(1-2t) \tag{26}$$

The above equation is for $c_i \neq 0$. As shown in Eq. (20), $\hat{g}_i(U_i) = a_i + b_i U_i$ when $c_i = 0$, where the normal variable U_i is involved. In this case, the CGF is given by

$$K_{Z_i}(t) = \tfrac{1}{2}t^2 \tag{27}$$

To use Eqs. (26) and (27), we rewrite Eq. (20) as

$$\hat{g}_i(U_i) \approx \begin{cases} e_i + \sigma_{Z_i}^2\left(\dfrac{Z_i}{\sigma_{Z_i}}\right)^2 & c_i > 0 \\ e_i - \sigma_{Z_i}^2\left(\dfrac{Z_i}{\sigma_{Z_i}}\right)^2 & c_i < 0 \\ a_i + b_i U_i & c_i = 0 \end{cases} \tag{28}$$

Our goal is to obtain the CGF of $\hat{g}(\mathbf{U})$. We then need to use the following properties of a CGF.

(1) If $Y = mX$, then $K_Y(t) = K_X(mt)$, where X and Y are random variables, $K_X(t)$ and $K_Y(t)$ are CGFs of X and Y, respectively, and m is a constant.
(2) If X and Y are independent, $K_{X+Y} = K_X(t) + K_Y(t)$, where $K_{X+Y}(t)$ is the CGF of $X+Y$.

Using the above properties and Eq. (28), we obtain the CGF of $\hat{g}_i(U_i)$,

$$K_{\hat{g}_i}(t) = \begin{cases} e_i t + \dfrac{\lambda_i \sigma_{Z_i}^2 t}{1-2\sigma_{Z_i}^2 t} - \dfrac{1}{2}\log(1-2\sigma_{Z_i}^2 t) & c_i > 0 \\ e_i t - \dfrac{\lambda_i \sigma_{Z_i}^2 t}{1-2\sigma_{Z_i}^2 t} - \dfrac{1}{2}\log(1+2\sigma_{Z_i}^2 t) & c_i < 0 \\ e_i t + \dfrac{1}{2}b_i t^2 & c_i = 0 \end{cases} \tag{29}$$

and finally the CGF of $\hat{g}(\mathbf{U})$

$$K_{\hat{g}}(t) \approx \sum_{i=1}^{n} K_{\hat{g}_i}(t) \tag{30}$$

3.5 Probability of Failure p_f. Once the CGF $K_{\hat{g}}(t)$ is available, the probability of failure p_f can be easily estimated by saddlepoint approximation [14]. At first, we obtain the saddlepoint t_s by solving

$$K'_{\hat{g}}(t) = q \tag{31}$$

where $K'_{\hat{g}}(t)$ is the derivative of $K_{\hat{g}}(t)$. Then, p_f is computed by [14,33–37]

$$p_f = \Phi(w) + \phi(w)\left(\frac{1}{w} - \frac{1}{v}\right) \tag{32}$$

where $\phi(\cdot)$ is the probability density function (PDF) of a standard normal distribution,

$$w = \mathrm{sgn}(t_s)\{2[t_s q - K_{\hat{g}}(t_s)]\}^{1/2} \tag{33}$$

and

$$v = t_s[K''_{\hat{g}}(t_s)]^{1/2} \tag{34}$$

where $\mathrm{sgn}(t_s) = +1, -1$, or 0, depending on whether t_s is positive, negative, or zero; $K''_{\hat{g}}(t_s)$ is the second derivative of $K_{\hat{g}}(t)$.

As shown in Ref. [37], the accuracy of the saddlepoint approximation is extremely high for p_f associated with the approximated function in Eq. (28). As a result, the accuracy of the SORM-FOE mostly depends on the accuracy of the quadratic approximation.

Downloaded From: http://mechanicaldesign.asmedigitalcollection.asme.org/ on 01/12/2016 Terms of Use: http://www.asme.org/about-asme/terms-of-use

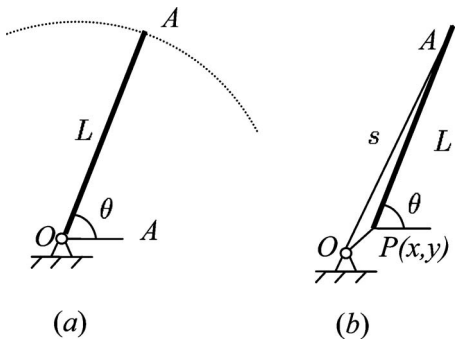

Fig. 3 A pinned rod

Since this approximation is generally more accurate than the linear approximation in the FORM, the SORM-FOE is, in general, more accurate than the FORM. Because the SORM-FOE requires one more point with n coordinate components, the total number of function calls is equal to that of the FORM plus n, namely,

$$N_{\text{SORM-FOE}} = N_{\text{MPP}} + n \tag{35}$$

3.6 Selection of the Step Size δ_i. As shown in Eq. (17), δ_i determines the location of the new point $\tilde{u}_i$. Because we prefer higher accuracy of the approximation near the MPP, δ_i should not be large. δ_i should also be determined by the importance of random variables at the MPP. We therefore use the following approach to set a value for δ_i,

$$\boldsymbol{\delta} = \delta \frac{\nabla \hat{g}(\mathbf{u}^*)}{\|\nabla \hat{g}(\mathbf{u}^*)\|} = \frac{\delta}{\|\nabla \hat{g}(\mathbf{u}^*)\|} \left(\frac{\partial \hat{g}(\mathbf{U})}{\partial U_1}, \ldots, \frac{\partial \hat{g}(\mathbf{U})}{\partial U_n} \right)\Bigg|_{\mathbf{u}^*} \tag{36}$$

where $\boldsymbol{\delta} = (\delta_1, \ldots, \delta_n)$, $\delta_i = (\delta / \|\nabla \hat{g}(\mathbf{u}^*)\|)(\partial \hat{g}(\mathbf{U}) / \partial U_i)|_{\mathbf{u}^*}$, and $\boldsymbol{\delta}$ is a scale factor.

In the above equation, $(1/\|\nabla \hat{g}(\mathbf{u}^*)\|)(\partial \hat{g}(\mathbf{U}) / \partial U_i)|_{\mathbf{u}^*}$ represents the sensitivity of the limit-state function to random variable U_i. Therefore, Eq. (36) indicates that the higher the sensitivity to a specific variable is, the larger the step size for that variable is. Realizing that a value of 1.0 means one standard deviation in the U-space, we recommend to set the scale factor δ_i to be 0.5–1.0. In all the examples that follow, we use $\delta_i = 1.0$. If the sensitivity is too small, for example, less than 10^{-6}, the effect of U_i on the limit-state function is negligible. To avoid any implementation difficulties, in this case, we delete U_i from the variable list and fix it to zero.

4 Numerical Example

Three problems are used to evaluate the SORM-FOE in terms of accuracy and efficiency. The first example clearly demonstrates the implementation procedure. Example 2 deals with a four-bar linkage mechanism with nine random variables. Example 3 shows the capability of the SORM-FOE for handling a structural analysis with a relatively large number of random variables (21 variables). The scale factor in Eq. (36) is taken as $\delta_i = 1.0$ for all the examples.

4.1 Example 1—A Pinned Rod Analysis. As shown in Fig. 3(*a*), the rod OA is pinned at the revolute joint O. The path of point A is a circle with a radius of $L = 10.0$ mm. A clearance of $r_c = 0.01$ mm at joint O exists because of the gap between the hole and the pin. The joint can be modeled as a virtual link OP, as shown in Fig. 3(*b*). Then, the position of A is given by

$$s = \sqrt{(L \sin\theta + x)^2 + (L \cos\theta + y)^2} \tag{37}$$

s should be close to L, but should not be greater than L. The required error q is set to 0.0099 mm. The limit-state function is therefore defined by

$$g(x,y) = s - L = \sqrt{(L \sin\theta + x)^2 + (L \cos\theta + y)^2} - L < -q \tag{38}$$

Let x and y be the coordinates of point P, and assume that the position of P is uniform within clearance r_c [38–40]. x and y are dependent because their joint PDF is

$$f_{x,y}(x,y) = \begin{cases} \dfrac{1}{\pi r_c^2} & \text{if } x^2 + y^2 \le r_c^2 \\ 0 & \text{otherwise} \end{cases} \tag{39}$$

The marginal PDF of x is given by

$$f_x(x) = \int_{-\infty}^{\infty} f_{xy}(x,y)dy = \int_{-\sqrt{r_c^2 - x^2}}^{\sqrt{r_c^2 - x^2}} \frac{1}{\pi r_c^2} dy = \frac{2\sqrt{r_c^2 - x^2}}{\pi r_c^2} (-r_c \le x \le r_c) \tag{40}$$

The marginal CDF of x is given by

$$F_x(x) = \int_{-\infty}^{x} f_x(x)dx = \int_{-\infty}^{x} \frac{2\sqrt{r_c^2 - x^2}}{\pi r_c^2} dx = \frac{1}{\pi r_c^2} \left(x\sqrt{r_c^2 - x^2} + r_c^2 \arcsin\frac{x}{r_c} \right) + \frac{1}{2} \tag{41}$$

The conditional PDF of y is given by

$$f_{y|x}(y|x) = \frac{f_{xy}(xy)}{f_x(x)} = \frac{1}{2} \frac{1}{\sqrt{r_c^2 - x^2}} (-r_c \le x \le r_c) \tag{42}$$

The conditional CDF of y is given by

$$f_{y|x}(y|x) = \int_{-\infty}^{y} f_{y|x}(y|x)dy = \frac{1}{2} \left(\frac{y}{\sqrt{r_c^2 - x^2}} + 1 \right) (-\sqrt{r_c^2 - x^2} \le y \le \sqrt{r_c^2 - x^2}, -r_c \le x \le r_c) \tag{43}$$

At first, we use the FORM to solve the problem. x and y are transformed into standard normal variables U_x and U_y. U_x is given by

$$\Phi(U_x) = F_x(x) = \frac{1}{\pi r_c^2} \left(x\sqrt{r_c^2 - x^2} + r_c^2 \arcsin\frac{x}{r_c} \right) + \frac{1}{2} \tag{44}$$

and U_y is given by

$$\Phi(U_y) = F_{y|x}(y|x) = \frac{1}{2} \left(\frac{y}{\sqrt{r_c^2 - x^2}} + 1 \right) \tag{45}$$

After the transformation, the MPP is found at $\mathbf{u}^* = (u_x^*, u_y^*) = (-1.8081, -2.1073)$. We then use MCS to confirm the solution. A large sample size of 10^8 is used to ensure that the MCS solution is accurate. The error of other methods with respect to the MCS solution is defined in

$$\text{Error } \% = \frac{p_f - \text{MCS solution}}{\text{MCS solution}} \times 100 \tag{46}$$

The results are given in Table 1. The error of the FORM is 358.7%. The reason for the large error is explained in Figs. 4 and 5. Figure 4 shows that the limit-state function in the X-space is near linear. However, Fig. 5 indicates that the limit-state function in the transformed U-space becomes highly nonlinear. The increased nonlinearity is due to the dependency between x and y and the nonlinear X-to-U transformation. The linearization in the U-space produces a large error.

The efficiency is measured by the number of limit-state function calls N, which include N_1 (the number of function calls for

Downloaded From: http://mechanicaldesign.asmedigitalcollection.asme.org/ on 01/12/2016 Terms of Use: http://www.asme.org/about-asme/terms-of-use

Table 1 p_f if x is transformed first

Method	p_f	Error (%)	N	N_1	N_2
FORM	2.7460×10^{-3}	358.7	36	36	–
SORM (Breitung)	8.5171×10^{-4}	42.3	39	36	3
SORM (Tvedt)	6.9148×10^{-4}	15.5	39	36	3
SORM-FOE	6.4571×10^{-4}	7.9	38	36	2
MCS	5.9865×10^{-4}	–	10^8	–	–

the MPP search) and N_2 (the number of function calls after the MPP search). The number of function calls of the FORM is 36 or $N_1=36$ and $N_2=0$.

We now look at the solution from the SORM. Both of the SORM methods are much more accurate than the FORM, but the error of the Breitung method is still relatively large. The number of function calls by the SORM is 39, higher than that of the FORM.

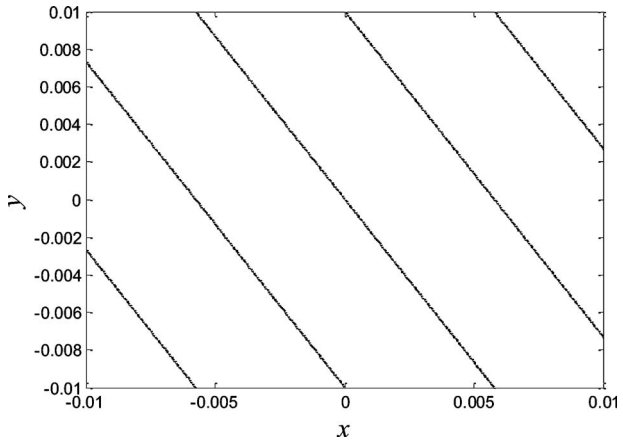

Fig. 4 Contours of the limit-state function in the X-space

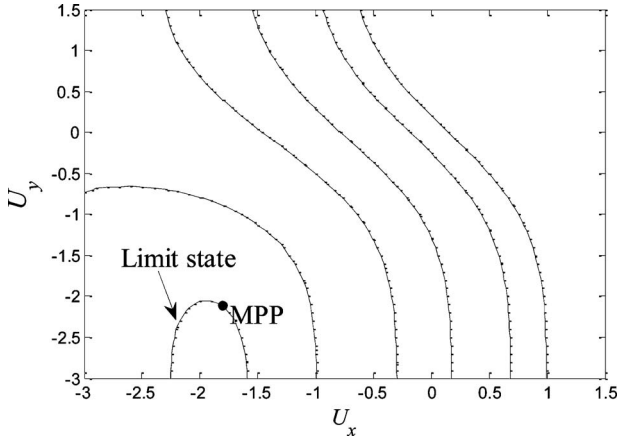

Fig. 5 Contours of the limit-state function in the U-space

We then apply the SORM-FOE. After the MPP search, two more points with $\tilde{u}_i=u_i^*+\delta_i$ $(i=x,y)$ are used for the following second-order approximation:

$$g(x,y)=\hat{g}(U_x,U_y)\approx\hat{g}_x(U_x)+\hat{g}_y(U_y)-(-q)\approx(a_x+b_xU_x+c_xU_x^2)+(a_y+b_yU_y+c_yU_y^2)+q \tag{47}$$

Then, the CGF of $\hat{g}(U_x,U_y)$, $K_{\hat{g}}$, is derived based on Eqs. (29) and (30). Solving for the saddlepoint with $K'_{\hat{g}}=q$ and using Eq. (32), we obtain p_f, As shown in Table 1, the SORM-FOE is much more accurate than the FORM and SORM.

The number of function calls of the SORM-FOE is 38, including 36 for the MPP search and 2 for the function evaluations at the additional point. Its efficiency gain over the SORM is not significant: Only one function call is saved. The reason is that there are only two random variables. As shown in example 3, for problems with more random variables, the former method will be much more efficient than the latter method.

In the above FORM analysis, x was transformed first followed by the transformation of y. If we transform y first and rework the problem, the results from the FORM and SORM-FOE will be different. The results are given in Table 2, which show that the SORM-FOE is still the most accurate method.

4.2 Example 2—Crank-Slider Mechanism Analysis. A crank-slider mechanism is shown in Fig. 6. R_2, R_3, and R_4 are the lengths of the mechanism. C_1, C_2, and C_3 are the clearance circles [39,41–46] at the three revolute joints. x_i and y_i are the x- and y-components of C_i $(i=1,2,3)$. With the same reason explained in example 1, we assume the locations of the joint centers to be uniform within the clearance radii r_{ci} $(i=1,2,3)$. The joint PDFs, the marginal PDFs, and the CDFs of the coordinates of the joints, x_i and y_i, have been derived in example 1 in Eqs. (39)–(43). The distributions are given in Tables 3 and 4.

The motion output is the displacement of the slider R_1. The loop-closure equations of the mechanism are given by

$$\begin{aligned} R_2\cos\theta_2+R_3\cos\theta_3-R_1+x_1+x_2-x_3=0\\ R_2\sin\theta_2+R_3\sin\theta_3-R_4+y_1+y_2-y_3=0\end{aligned} \tag{48}$$

R_1 can then be solved from the above equations and is given by

$$Y=R_1=g(\mathbf{X})=g(R_2,R_3,R_4,x_1,y_1,x_2,y_2,x_3,y_3;\theta_2) \tag{49}$$

Table 2 p_f if y is transformed first

Method	p_f	Error (%)	N	N_1	N_2
FORM	4.4445×10^{-3}	642.4	210	210	–
SORM (Breitung)	6.0542×10^{-5}	−89.9	213	210	3
SORM (Tvedt)	4.7485×10^{-5}	−92.1	213	210	3
SORM-FOE	6.3084×10^{-4}	5.4	212	210	2
MCS	5.9865×10^{-4}	–	10^8	–	–

Downloaded From: http://mechanicaldesign.asmedigitalcollection.asme.org/ on 01/12/2016 Terms of Use: http://www.asme.org/about-asme/terms-of-use

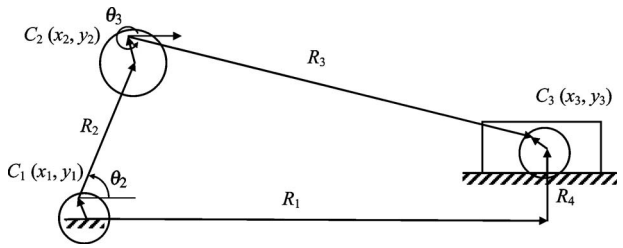

Fig. 6 Crank-slider mechanism

Table 3 Random dimensions

Variable	Mean (mm)	Standard deviation (mm)	Distribution
R_2	$\mu_2=100.0$	$\sigma_2=0.01$	Normal
R_3	$\mu_3=150.0$	$\sigma_3=0.01$	Normal
R_4	$\mu_4=50.0$	$\sigma_4=0.01$	Normal

Table 4 Random clearances

Variable	Clearance radius r_c (mm)	Distribution
(x_1, y_1)	0.012	2D uniform within a circle
(x_2, y_2)	0.012	2D uniform within a circle
(x_3, y_3)	0.012	2D uniform within a circle

Because of the randomness in the dimension and clearance parameters, the actual position of the slider will be different from its nominal position. Suppose a failure is defined by the event $|R_1 - \bar{R}_1| > q$, where q is the required error that is set to 0.05 mm, and $\bar{R}$ is the nominal position that is determined by the mean values of the dimension and clearance parameters. We then define the performance function as

$$g = R_1 - \bar{R}_1 \tag{50}$$

A failure occurs when $g > q$ $(R_1 > \bar{R}_1 + q)$ or $q < -q$ $(R_1 < \bar{R}_1 - q)$. Then, the probability of failure is

$$p_f = p_{f1} + p_{f2} = \Pr\{g > q\} + \Pr\{g < -q\} \tag{51}$$

where $p_{f1} = \Pr\{g > q\}$ and $p_{f2} = \Pr\{g < -q\}$.

The probabilities of failure over $\theta_2 = [10°, 90°]$ are plotted in Fig. 7 and listed in Table 5. The sample size of MCS is 10^8. The errors of all the methods are shown in Table 6 along with the numbers of function calls in Table 7. The results indicate that the SORM-FOE produces the most accurate solution. The FORM significantly overpredicts p_f, and the SORM underpredicts p_f. The numbers of function calls by the SORM-FOE is slightly larger than those of the FORM but are much less than those of the SORM. In this problem, there are nine random variables ($n=9$) and two limit-state functions $g > q$ and $g < -q$; therefore, the SORM-FOE calls the limit-state functions 18 more times ($2n = 2 \times 9 = 18$ according to Eq. (35)) than the FORM does, whereas the SORM calls the limit-state functions 90 more times ($2\left(\frac{n(n+1)}{2}\right) = 2 \times \left(\frac{9\times(9+1)}{2}\right) = 90$ according to Eq. (10)) than the FORM does.

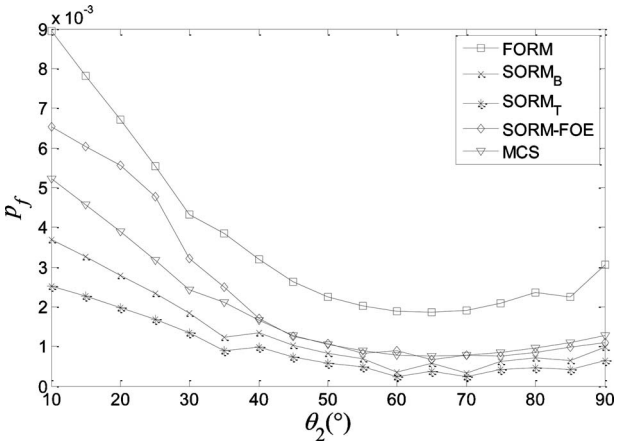

Fig. 7 p_f over $\theta_2 = [10\ \text{deg}, 90\ \text{deg}]$

Table 6 Error (%)

θ_2 (deg)	FORM	SORM (Breitung)	SORM (Tvedt)	SORM-FOE
10	71.6	−29.1	−51.7	25.2
20	72.4	−28.4	−49.5	42.6
30	78.8	−23.5	−44.2	33.0
40	93.3	−18.3	−40.2	3.8
50	111.9	−22.8	−45.6	2.5
60	138.8	−56.6	−70.5	14.8
70	147.8	−56.6	−70.5	0.2
80	146.5	−24.8	−51.1	−12.4
90	138.2	−22.6	−49.5	−14.7

4.3 Example 3—A Cantilever Beam Analysis [47]. The cantilever beam in Fig. 8 is subjected to external forces F_1 and F_2, external moments M_1 and M_2, and external distributed loads represented by (q_{L1}, q_{R1}) and (q_{L2}, q_{R2}). Other variables are the dimensions of the beam, the locations of the loading, the yield strength S, and the maximal allowable shear stress $\tau_{\max}$. The distributions of these 21 random variables are listed in Table 8.

Table 5 p_f for the crank-slider mechanism

θ_2 (deg)	FORM	SORM (Breitung)	SORM (Tvedt)	SORM-FOE	MCS
10	8.9455×10^{-3}	3.6960×10^{-3}	2.5190×10^{-3}	6.5261×10^{-3}	5.2121×10^{-3}
20	6.7210×10^{-3}	2.7932×10^{-3}	1.9677×10^{-3}	5.5657×10^{-3}	3.8988×10^{-3}
30	4.3231×10^{-3}	1.8490×10^{-3}	1.3490×10^{-3}	3.2160×10^{-3}	2.4180×10^{-3}
40	3.1867×10^{-3}	1.3477×10^{-3}	9.8606×10^{-4}	1.7120×10^{-3}	1.6487×10^{-3}
50	2.2384×10^{-3}	8.1612×10^{-4}	5.7435×10^{-4}	1.0825×10^{-3}	1.0565×10^{-3}
60	1.8741×10^{-3}	3.4089×10^{-4}	2.3168×10^{-4}	9.0061×10^{-4}	7.8480×10^{-4}
70	1.9091×10^{-3}	3.3439×10^{-4}	2.2723×10^{-4}	7.7170×10^{-4}	7.7050×10^{-4}
80	2.3491×10^{-3}	7.1654×10^{-4}	4.6559×10^{-4}	8.3526×10^{-4}	9.5300×10^{-4}
90	3.0502×10^{-3}	9.9093×10^{-4}	6.4643×10^{-4}	1.0920×10^{-3}	1.2807×10^{-3}

Downloaded From: http://mechanicaldesign.asmedigitalcollection.asme.org/ on 01/12/2016 Terms of Use: http://www.asme.org/about-asme/terms-of-use

Table 7 Numbers of function evaluations

θ_2 (deg)	N			N_1	N_2	
	FORM	SORM	SORM-FOE		SORM	SORM-FOE
10	488	578	506	488	90	18
20	274	364	292	274	90	18
30	744	834	762	744	90	18
40	285	375	303	285	90	18
50	375	465	393	375	90	18
60	446	536	464	446	90	18
70	992	1082	1010	992	90	18
80	292	382	310	292	90	18
90	334	424	352	334	90	18

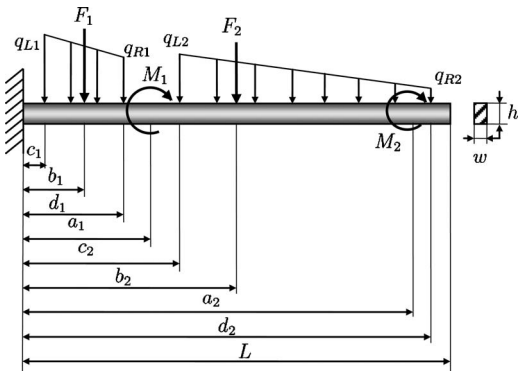

Fig. 8 A cantilever beam

Table 8 Random variables

	Random variable	Mean value	Standard deviation	Distribution type
1	M_1 (N m)	50.0×10^3	5.0×10^3	Normal
2	M_2 (N m)	30.0×10^3	3.0×10^3	Normal
3	F_1 (N)	18.0×10^3	4.0×10^3	Extreme value type I
4	F_2 (N)	30.0×10^3	3.0×10^3	Normal
5	q_{L1} (N/m)	30.0×10^3	1.0×10^3	Normal
6	q_{R1} (N/m)	20.0×10^3	1.0×10^3	Normal
7	q_{L2} (N/m)	20.0×10^3	1.0×10^3	Normal
8	q_{R2} (N/m)	1.0×10^3	10.0	Normal
9	a_1 (m)	1.5	0.005	Normal
10	a_2 (m)	4.5	0.005	Normal
11	b_1 (m)	0.75	0.001	Normal
12	b_2 (m)	2.50	0.001	Normal
13	c_1 (m)	0.25	0.0005	Normal
14	c_2 (m)	1.75	0.001	Normal
15	d_1 (m)	1.25	0.001	Normal
16	d_2 (m)	4.75	0.001	Normal
17	L (m)	5.0	0.01	Normal
18	w (m)	0.2	0.0001	Normal
19	h (m)	0.4	0.0001	Normal
20	S (Pa)	80.0×10^6	10.0×10^6	Normal
21	τ_{max} (Pa)	3.5×10^6	0.5×10^6	Normal

The first limit-state function represents the difference between the maximum normal stress and the yield strength. The function is given by

$$g_1(x) = 6\frac{M}{wh^2} - S \tag{52}$$

where the bending moment M at the root is

$$M = \sum_{i=1}^{2} M_i + \sum_{i=1}^{2} F_i b_i + \sum_{i=1}^{2} q_{Li}(d_i - c_i)(d_i + c_i)/2 - \sum_{i=1}^{2} [(q_{Ri} - q_{Li}) \times (d_i - c_i)/2][c_i + 2(d_i - c_i)/3] \tag{53}$$

The second limit-state function is defined as the difference between the maximum shear stress and the allowable shear stress and is given by

$$g_2(x) = \frac{3Q}{2wh} - \tau_{max} \tag{54}$$

where the shear force at the root is

$$Q = \sum_{i=1}^{2} F_i + \sum_{i=1}^{2} q_{Li}(d_i - c_i) + \sum_{i=1}^{2} (q_{Ri} - q_{Li})(d_i - c_i)/2 \tag{55}$$

The analysis results are given in Tables 9 and 10, which show that the SORM-FOE is more accurate than the FORM, and the SORM-FOE is also much more efficient than the SORM. As expected, the SORM-FOE may not be as accurate as the SORM. For example, the error of the former method is slightly larger than the second method (SORM-Breitung) for g_1. The SORM-FOE is much more efficient than the SORM.

5 Conclusions

The SORM-FOE uses a second-order approximation to the original limit-state function. The approximation is achieved by decomposing the limit-state function with additive univariate functions at the MPP. Each of the univariate functions is further approximated as a quadratic function. This is performed by using the gradient of the limit-state function at the MPP and one new point along the line of the random variable that is involved in the univariate function.

Because of its second-order approximation, the accuracy of the SORM-FOE is, in general, higher than that of the FORM. The efficiency of the SORM-FOE is slightly lower than that of the FORM. The additional computational cost is equivalent to one gradient evaluation in the MPP search. The error of the presented method, however, will be large if the univariate dimension reduction does not accurately approximate the limit-state function [5–13].

The SORM-FOE is based on the FORM, and both of the methods cannot directly deal with multiple MPPs [48]. For this situation, we can apply the SORM-FOE at all the MPPs and then create quadratic functions at the MPPs. The saddlepoint approximation-based system reliability method [47] can then be extended to accommodate quadratic functions. Because one limit-state function is involved, the SORM-FOE is applicable for only

Table 9 p_f for g_1

Method	p_f	Error (%)	N	N_1	N_2
FORM	2.5133×10^{-4}	−2.82	331	331	–
SORM (Breitung)	2.5840×10^{-4}	−0.09	562	331	231
SORM (Tvedt)	2.6222×10^{-4}	1.38	562	331	231
SORM-FOE	2.5892×10^{-4}	0.109	352	331	21
MCS	2.5864×10^{-4}	–	10^8	–	–

Downloaded From: http://mechanicaldesign.asmedigitalcollection.asme.org/ on 01/12/2016 Terms of Use: http://www.asme.org/about-asme/terms-of-use

Table 10 p_f for g_2

Method	p_f	Error (%)	N	N_1	N_2
FORM	1.1495×10^{-3}	−10.0	309	309	–
SORM (Breitung)	1.2639×10^{-3}	−1.06	540	309	231
SORM (Tvedt)	1.3284×10^{-3}	−3.99	540	309	231
SORM-FOE	1.2768×10^{-3}	−0.04	330	309	21
MCS	1.2774×10^{-3}	–	10^8	–	–

component reliability analysis. It can be extended to a system reliability analysis, and such an extension needs further investigation.

Acknowledgment

We would like to thank the support from Xihua University to J. Z. for his stay as a Visiting Scholar at the Missouri University of Science and Technology.

References

[1] Wu, Y. T., Millwater, H. R., and Cruse, T. A., 1990, "Advanced Probabilistic Structural Analysis Method for Implicit Performance Functions," AIAA J., **28**(9), pp. 1663–1669.
[2] Hasofer, A. M., and Lind, N. C., 1974, "An Exact and Invariant First-Order Reliability Format," J. Engrg. Mech. Div., **100**, pp. 111–121.
[3] Hohenbichler, M., and Rackwitz, R., 1983, "First-Order Concepts in System Reliability," Struct. Safety, **1**(3), pp. 177–188.
[4] Breitung, K., 1984, "Asymptotic Approximations for Multinormal Integrals," J. Eng. Mech., **110**(3), pp. 357–366.
[5] Li, G., Rosenthal, C., and Rabitz, H., 2001, "High Dimensional Model Representations," J. Phys. Chem. A, **105**(33), pp. 7765–7777.
[6] Demiralp, M., 2009, "High Dimensional Model Representation Supported by Products of Univariate Functions," International Conference on Numerical Analysis and Applied Mathematics, Vol. 1168, pp. 420–423.
[7] Rahman, S., 2009, "Extended Polynomial Dimensional Decomposition for Arbitrary Probability Distributions," J. Eng. Mech., **135**(12), pp. 1439–1451.
[8] Rahman, S., and Xu, H., 2004, "A Univariate Dimension-Reduction Method for Multi-Dimensional Integration in Stochastic Mechanics," Probab. Eng. Mech., **19**(4), pp. 393–408.
[9] Xu, H., and Rahman, S., 2004, "A Generalized Dimension-Reduction Method for Multidimensional Integration in Stochastic Mechanics," Int. J. Numer. Methods Eng., **61**(12), pp. 1992–2019.
[10] Yook, S., Min, J., Kim, D. H., and Choi, D. H., 2009, "Reliability Analysis Using Dimension Reduction Method With Variable Sampling Points," Transactions of the Korean Society of Mechanical Engineers, A, **33**(9), pp. 870–877.
[11] Rahman, S., and Wei, D., 2006, "A Univariate Approximation at Most Probable Point for Higher-Order Reliability Analysis," Int. J. Solids Struct., **43**(9), pp. 2820–2839.
[12] Lee, I., Choi, K. K., Du, L., and Gorsich, D., 2008, "Inverse Analysis Method Using MPP-Based Dimension Reduction for Reliability-Based Design Optimization of Nonlinear and Multi-Dimensional Systems," Comput. Methods Appl. Mech. Eng., **198**(1), pp. 14–27.
[13] Wei, D., and Rahman, S., 2007, "Structural Reliability Analysis by Univariate Decomposition and Numerical Integration," Probab. Eng. Mech., **22**(1), pp. 27–38.
[14] Huang, B., and Du, X., 2006, "Uncertainty Analysis by Dimension Reduction Integration and Saddlepoint Approximations," ASME J. Mech. Des., **128**(1), pp. 26–33.
[15] Du, X., and Chen, W., 2004, "Sequential Optimization and Reliability Assessment Method for Efficient Probabilistic Design," ASME J. Mech. Des., **126**(2), pp. 225–233.
[16] Du, X., Guo, J., and Beeram, H., 2008, "Sequential Optimization and Reliability Assessment for Multidisciplinary Systems Design," Struct. Multidiscip. Optim., **35**(2), pp. 117–130.
[17] Hohenbichler, M., and Rackwitz, R., 1981, "Non-Normal Dependent Vectors in Structural Safety," J. Engrg. Mech. Div., **107**(6), pp. 1227–1238.
[18] Lee, I., Choi, K. K., and Gorsich, D., 2010, "System Reliability-Based Design Optimization Using the MPP-Based Dimension Reduction Method," Struct. Multidiscip. Optim., **41**(6), pp. 823–839.
[19] Youn, B. D., and Choi, K. K., 2004, "An Investigation of Nonlinearity of Reliability-Based Design Optimization Approaches," ASME J. Mech. Des., **126**(3), pp. 403–411.
[20] Youn, B. D., and Choi, K. K., 2004, "Selecting Probabilistic Approaches for Reliability-Based Design Optimization," AIAA J., **42**(1), pp. 124–131.
[21] Youn, B. D., Choi, K. K., and Du, L., 2005, "Enriched Performance Measure Approach for Reliability-Based Design Optimization," AIAA J., **43**(4), pp. 874–884.
[22] Tu, J., Choi, K. K., and Park, Y. H., 1999, "A New Study on Reliability-Based Design Optimization," ASME J. Mech. Des., **121**(4), pp. 557–564.
[23] Liang, J., Mourelatos, Z. P., and Nikolaidis, E., 2007, "A Single-Loop Approach for System Reliability-Based Design Optimization," ASME J. Mech. Des., **129**(12), pp. 1215–1224.
[24] Agarwal, H., Mozumder, C. K., Renaud, J. E., and Watson, L. T., 2007, "An Inverse-Measure-Based Unilevel Architecture for Reliability-Based Design Optimization," Struct. Multidiscip. Optim., **33**(3), pp. 217–227.
[25] Chiralaksanakul, A., and Mahadevan, S., 2007, "Decoupled Approach to Multidisciplinary Design Optimization Under Uncertainty," Optim. Eng., **8**(1), pp. 21–42.
[26] Mcdonald, M., and Mahadevan, S., 2008, "Design Optimization With System-Level Reliability Constraints," ASME J. Mech. Des., **130**(2), p. 021403.
[27] Rosenblatt, M., 1952, "Remarks on a Multivariate Transformation," Ann. Math. Stat., **23**(3), pp. 470–472.
[28] Lin, P. T., Gea, H. C., and Jaluria, Y., 2009, "A Modified Reliability Index Approach for Reliability-Based Design Optimization," Proceedings of the ASME 2009 International Design Engineering Technical Conferences and Computers and Information in Engineering Conference, IDETC/CIE 2009, San Diego, CA, Paper No. DETC 2009-87804.
[29] Zhang, Y., and Kiureghian, A. D., 1995, "Two Improved Algorithms for Reliability Analysis," R. Rackwitz, G. Augusti, and G. Borri, Editors, *Proceedings of the Sixth IFIP WG 7.5 Conference*, Assisi, 1994, Chapman and Hall, London, pp. 297–304.
[30] Tvedt, L., 1983, "Two Second-Order Approximations to the Failure Probability," Det Norske Veritas, Technical Report No. RDIV/20-004083.
[31] Zhao, Y. G., and Ono, T., 1999, "New Approximations for SORM: Part 1," J. Eng. Mech., **125**(1), pp. 79–85.
[32] Johnson, N., Kotz, S., and Balakrishnan, N., 1994, *Continuous Univariate Distributions*, 2nd ed., Wiley, New York, Vol. 1.
[33] Daniels, H., 1954, "Saddlepoint Approximations in Statistics," Ann. Math. Stat., **25**(4), pp. 631–650.
[34] Goutis, C., and Casella, G., 1999, "Explaining the Saddlepoint Approximation," Am. Stat., **53**(3), pp. 216–224.
[35] Huzurbazar, S., 1999, "Practical Saddlepoint Approximations," Am. Stat., **53**(3), pp. 225–232.
[36] Lugannani, R., and Rice, S., 1980, "Saddle Point Approximation for the Distribution of the Sum of Independent Random Variables," Adv. Appl. Probab., **12**(2), pp. 475–490.
[37] Huang, B., and Du, X., 2008, "Probabilistic Uncertainty Analysis by Mean-Value First Order Saddlepoint Approximation," Reliab. Eng. Syst. Saf., **93**(2), pp. 325–336.
[38] Rao, S. S., and Bhatti, P. K., 2001, "Probabilistic Approach to Manipulator Kinematics and Dynamics," Reliab. Eng. Syst. Saf., **72**(1), pp. 47–58.
[39] Tsai, M. J., and Lai, T. H., 2008, "Accuracy Analysis of a Multi-Loop Linkage With Joint Clearances," Mech. Mach. Theory, **43**(9), pp. 1141–1157.
[40] Choubey, M., and Rao, A. C., 1982, "Synthesizing Linkages With Minimal Structural and Mechanical Error Based Upon Tolerance Allocation," Mech. Mach. Theory, **17**(2), pp. 91–97.
[41] Choi, J. H., Lee, S. J., and Choi, D. H., 1998, "Stochastic Linkage Modeling for Mechanical Error Analysis of Planar Mechanisms," Mech. Struct. Mach., **26**(3), pp. 257–276.
[42] Mallik, A. K., and Dhande, S. G., 1987, "Analysis and Synthesis of Mechanical Error in Path-Generating Linkages Using a Stochastic Approach," Mech. Mach. Theory, **22**(2), pp. 115–123.
[43] Zhu, J., and Ting, K. L., 2000, "Uncertainty Analysis of Planar and Spatial Robots With Joint Clearances," Mech. Mach. Theory, **35**(9), pp. 1239–1256.
[44] Chakraborty, J., 1975, "Synthesis of Mechanical Error in Linkages," Mech. Mach. Theory, **10**(2–3), pp. 155–165.
[45] Xu, W., and Zhang, Q., 1989, "Probabilistic Analysis and Monte Carlo Simulation of the Kinematic Error in a Spatial Linkage," Mech. Mach. Theory, **24**(1), pp. 19–27.
[46] Chatterjee, G. B., and Mallik, A. K., 1987, "Mechanical Error of a Four-Bar Linkage Coupler Curve," Mech. Mach. Theory, **22**(1), pp. 85–88.
[47] Du, X., 2010, "System Reliability Analysis With Saddlepoint Approximation," Struct. Multidiscip. Optim., **42**(2), pp. 193–208.
[48] Der Kiureghian, A., and Dakessian, T., 1998, "Multiple Design Points in First and Second-Order Reliability," Struct. Safety, **20**(1), pp. 37–49.

Downloaded From: http://mechanicaldesign.asmedigitalcollection.asme.org/ on 01/12/2016 Terms of Use: http://www.asme.org/about-asme/terms-of-use